ACS Macro Letters

pubs.acs.org/macroletters

Letter

Elucidating the Impact of Hydrophilic Segments on ^{19}F MRI Sensitivity of Fluorinated Block Copolymers

Yiqing Wang, Xiao Tan, Adil Usman, Yuhao Zhang, Michał Sawczyk, Petr Král, Cheng Zhang,* and Andrew K. Whittaker*

Cite This: *ACS Macro Lett.* 2022, 11, 1195−1201

Read Online

ACCESS | Metrics & More | Article Recommendations | Supporting Information

ABSTRACT: A major challenge in the preparation of polymeric ^{19}F magnetic resonance imaging (MRI) contrast agents (CAs) is signal attenuation caused by reduced segmental mobility of partly fluorinated polymers possessing large numbers of fluorine atoms. Previous studies have thus mainly focused on the development of fluorinated segments for improved ^{19}F MRI; however, detailed investigations of the role of hydrophilic segments on imaging performance remain scarce. In this study, three hydrophilic and biocompatible monomers, i.e., 2-(methylsulfinyl)ethyl acrylate (MSEA), oligo(ethylene glycol) methyl ether acrylate (OEGA), and oligo(2-methyl-2-oxazoline) acrylate (OMOXA), were used to prepare perfluoropolyether (PFPE)-containing amphiphilic block polymers through reversible addition−fragmentation chain-transfer (RAFT) polymerization. The effect of the different hydrophilic segments on ^{19}F imaging performance was explored. The three polymers could be readily dissolved in aqueous solutions, forming assemblies with the hydrophobic PFPE as the core and the hydrophilic chains as the shell. Molecular dynamics simulations demonstrate that the POMOXA chains adopt a rigid, extended conformation, leading to a relatively short ^{19}F NMR spin−spin relaxation time (T_2), lower NMR detectable ^{19}F spins (i.e., visibility), and the least intense ^{19}F MRI signal. In contrast, although PMSEA−PFPE has a shorter ^{19}F NMR T_2 than POEGA−PFPE, the much higher ^{19}F spin visibility enhances its MRI signal intensity. The result confirms the importance of maintaining both high fluorine visibility and long T_2 relaxation time to prepare effective CAs and highlight the key role of the nonfluorinated hydrophilic segments in determining these parameters.

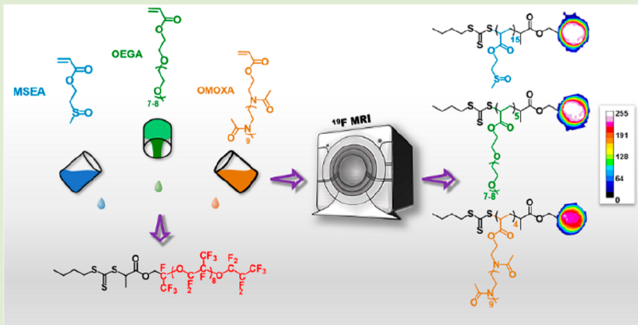

Magnetic resonance imaging (MRI) is widely used in medical diagnosis and drug development as a non-invasive technology for the visualization, characterization, and quantification of biological processes.[1−4] Conventional ^{1}H MRI acquires signals from the mobile protons present in organisms or materials.[5] However, the intense background signal from endogenous water molecules often makes it difficult to clearly identify diseased tissue, indicating the importance and urgency of developing new MRI agents based on different nuclei.[6−8]

^{19}F MRI, in which the signal arises only from administered fluorinated molecules, possesses a critical advantage over ^{1}H MRI in that no background signal can be detected due to the low concentration of mobile fluorine atoms in the body.[9−12] An important design requirement for effective ^{19}F contrast agents (CAs) is high ^{19}F content for ready detection by ^{19}F MRI. However, fluorine is hydrophobic in nature, and fluorocarbons tend to aggregate in aqueous solutions, which leads to attenuation of the ^{19}F MR signal and reduced imaging sensitivity.[13−15] A promising strategy to overcome the hydrophobicity of fluorine is to introduce hydrophilic segments to stabilize fluorine-containing polymers in aqueous solution.[14,16] Our team has successfully prepared a series of amphiphilic copolymers containing perfluoropolyether (PFPE) segments, having the highest fluorine content reported for polymeric ^{19}F MRI contrast agents.[17−21] A number of hydrophilic polymers can be used to stabilize PFPE in aqueous solution, including poly(ethylene glycol), polyoxazolines, and sulfinyl-containing polymers; however, the effect of different hydrophilic polymers on the segmental mobility of PFPE, and therefore the ^{19}F NMR properties and MR imaging performance, has not been studied in detail.[13,18,22]

In this study, we confirm through a combination of synthesis, characterization, and molecular dynamics simulations that the structure of the hydrophilic component of PFPE block copolymer ^{19}F MRI CAs can have a significant impact on ^{19}F NMR and MRI properties. Hydrophilic segments with

Received: July 15, 2022
Accepted: September 12, 2022

https://doi.org/10.1021/acsmacrolett.2c00414
ACS Macro Lett. 2022, 11, 1195−1201

Scheme 1. Synthetic Scheme Describing the Synthesis of the Three PFPE Block Copolymers, PMSEA–PFPE, POEGA–PFPE, and POMOXA–PFPE

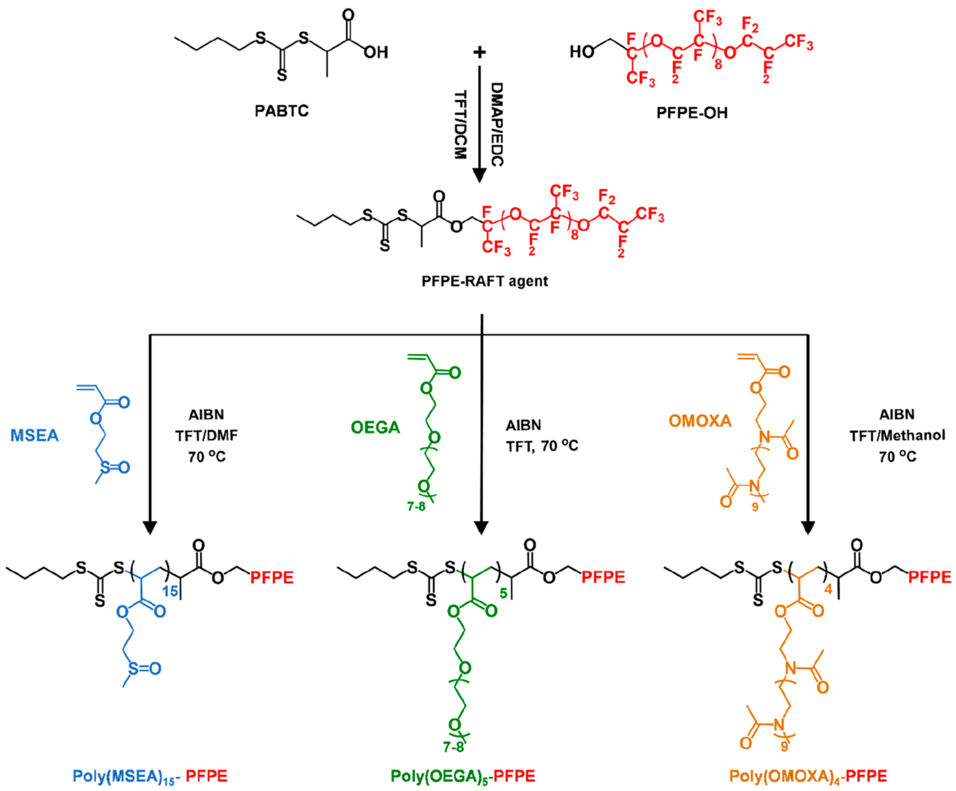

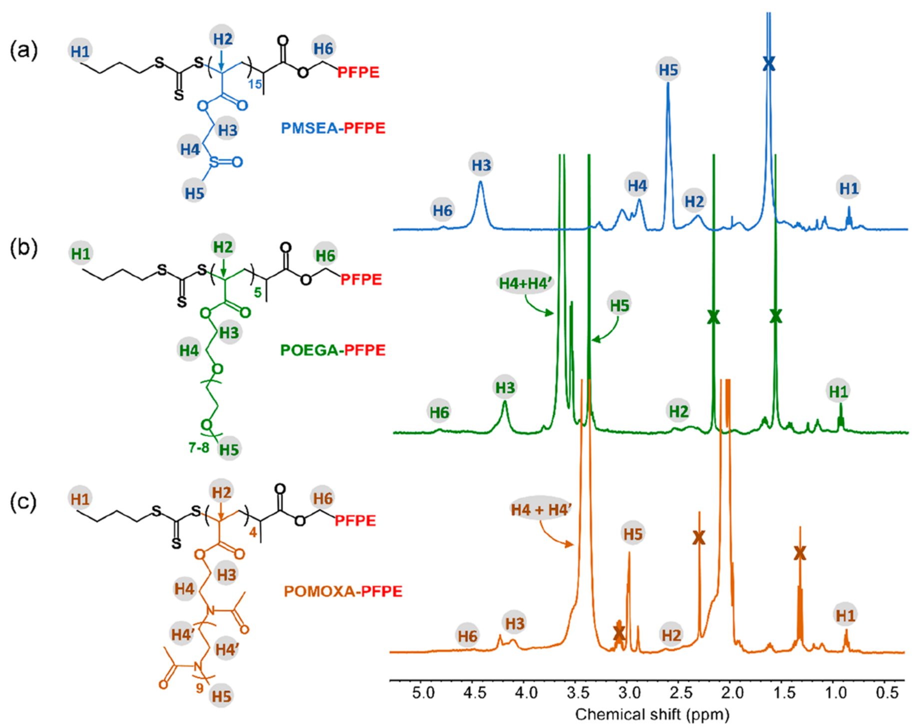

Figure 1. Chemical structures and assigned ^{1}H NMR spectra of (a) PMSEA–PFPE, (b) POEGA–PFPE, and (c) POMOXA–PFPE in $CDCl_3$.

varying hydrophilicity and molecular size, namely, (2-(methylsulfinyl)ethyl acrylate (MSEA), oligo(ethylene glycol) methyl ether acrylate (OEGA), and oligo(2-methyl-2-oxazoline) acrylate (OMOXA), were examined. Our results highlight that the hydrophilic segment can impact the assembly and conformation of PFPE CAs in aqueous solution and directly affect the ^{19}F NMR and MRI performance. The study reveals that both ^{19}F NMR relaxation times and NMR visibility, key

https://doi.org/10.1021/acsmacrolett.2c00414
ACS Macro Lett. 2022, 11, 1195–1201

Table 1. Detailed Structural Characteristics and ^{19}F NMR and ^{19}F MRI Properties of the Polymers (PMSEA−PFPE, POEGA−PFPE, and POMOXA−PFPE)

	conv. (%)	fluorine content (wt %)[a]	$M_{n,NMR}$ (g/mol)[b]	$M_{n,SEC}$ (g/mol)[c]	$Đ$[c]	D_h (nm)[d] DLS	^{19}F NMR T_1 (ms)[e]	^{19}F NMR T_2 (ms)[e]	^{19}F MRI SNR[f]
PMSEA−PFPE	86.3	22.5	4000	16500	1.05	9.3	373.3	41.3	222.0
POEGA−PFPE	89.0	22.7	3900	16000	1.04	7.5	375.4	62.3	213.5
POMOXA−PFPE	80.0	16.9	5300	17500	1.17	8.0	401.2	33.9	136.9

[a]The weight percentage of fluorine in the samples. [b]The $M_{n,NMR}$ for the polymers was calculated by considering the integrals of the peaks due to protons H3 (2H) and protons H1 (3H) as shown in Figure 1. [c]The $M_{n,SEC}$ and $Đ$ were obtained by size exclusion chromatography (SEC) in DMF. Note: the $M_{n,SEC}$ values were determined using polystyrene as an internal reference and are larger than $M_{n,NMR}$. [d]D_h was obtained by DLS (number-based) in PBS. [e]The ^{19}F NMR T_1/T_2 were measured in PBS/D_2O (90:10, v/v) at 298 K at 9.4 T. [f]The SNR value was calculated from the ^{19}F MR images at a ^{19}F concentration of 6.8 mg/mL.

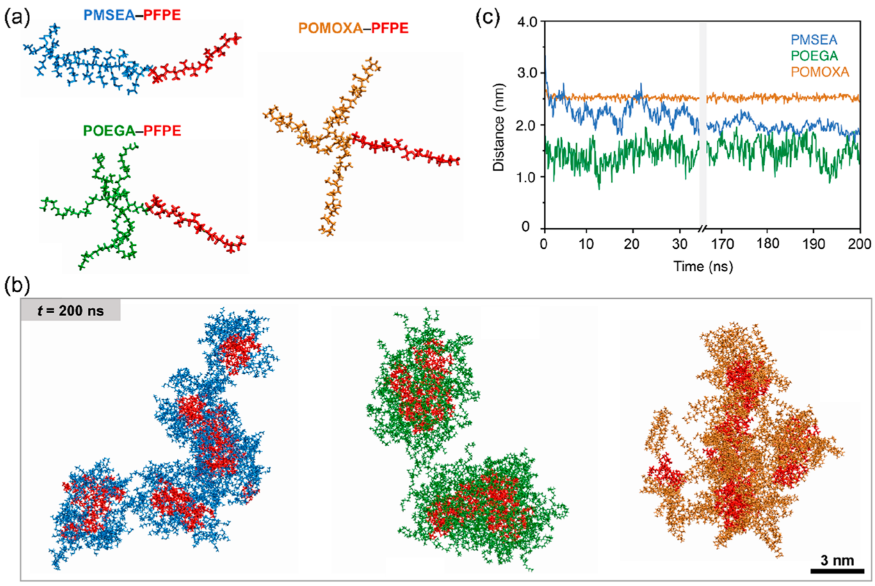

Figure 2. Snapshots from the MD simulations of the self-assembly behavior of 40 polymer chains in 150 mM NaCl solution. (a) Initial structures of each single PMSEA−PFPE, POEGA−PFPE, and POMOXA−PFPE chain. The PFPE segments are shown in red, surrounded by hydrophilic monomer units in blue, green, or orange. (b) Assemblies formed after 200 ns simulation time, from left to right: PMSEA−PFPE, POEGA−PFPE, and POMOXA−PFPE, respectively. (c) The average distance between terminal fragments of hydrophilic chains and the branching site at the polymer backbone.

parameters for the design and synthesis of effective ^{19}F MRI CAs,[23] are sensitive to the choice of hydrophilic segments.

In this study, we report the syntheses and characterization of a series of amphiphilic block copolymers containing PFPE as ^{19}F MRI contrast agents. In these block copolymers, the hydrophilic segments are varied as polymers of MSEA, OEGA, and OMOXA to investigate the relationship between molecular structure and imaging performance. An oligomeric PFPE RAFT agent was prepared by a dicyclohexylcarbodiimide/4-(dimethylamino)pyridine (EDCl/DMAP) esterification coupling reaction between (propionic acid)yl butyl trithiocarbonate (PABTC) and hydroxy-terminated PFPE ($M_n \approx 1300$ g/mol, Scheme 1).[24] Figure S1 shows the ^{1}H and ^{19}F NMR spectra of PABTC−PFPE macro-CTA in $CDCl_3$. All of the peaks in both the ^{1}H and ^{19}F NMR spectra can be successfully assigned. More specifically, in the ^{1}H NMR spectrum, a multiplet at ∼4.6 ppm (H7, Figure S1) appears after esterification, corresponding to the methylene protons adjacent to the PFPE segment, confirming the successful synthesis of the PABTC−PFPE macro-CTA. In the ^{19}F NMR spectrum in Figure S1, the intense resonance at ∼−80 ppm is due to the fluorinated methyl and methylene groups in the repeat unit of the PFPE oligomer.

Three block copolymers, poly(MSEA)$_{15}$-PFPE (PMSEA−PFPE), poly(OEGA)$_5$-PFPE (POEGA−PFPE), and poly(OMeOx$_{10}$A)$_4$-PFPE (POMOXA-PFPE), were prepared via RAFT polymerization. The degrees of polymerization (DP) of the hydrophilic MSEA, OEGA, and OMOXA monomers were controlled to be 15, 5, and 4, respectively, to obtain a similar fluorine content in the three block copolymers. The conversion of monomers to polymers was determined by ^{1}H NMR from integration of the peaks due to a residual monomer at ∼6.5 ppm (peak a, 1H) and the newly formed polymer peaks at ∼4.5 ppm (peak b, 2H) in the ^{1}H NMR spectra of the crude solution mixtures (Figure S2). The ^{1}H spectra of the three polymers after purification are shown in Figure 1. In the spectrum of PMSEA−PFPE (Figure 1a), the methylene protons (2H, $-CH_2O-$) adjacent to the ester groups of the MSEA and the terminal ether oxygen of PFPE appear at ∼4.2 ppm (H3) and ∼4.6 ppm (H6), respectively. In addition, the ^{19}F NMR spectra of the three polymers can be successfully assigned based on previous reports, and the integrated intensities of each peak correspond well to the number of

https://doi.org/10.1021/acsmacrolett.2c00414
ACS Macro Lett. 2022, 11, 1195−1201

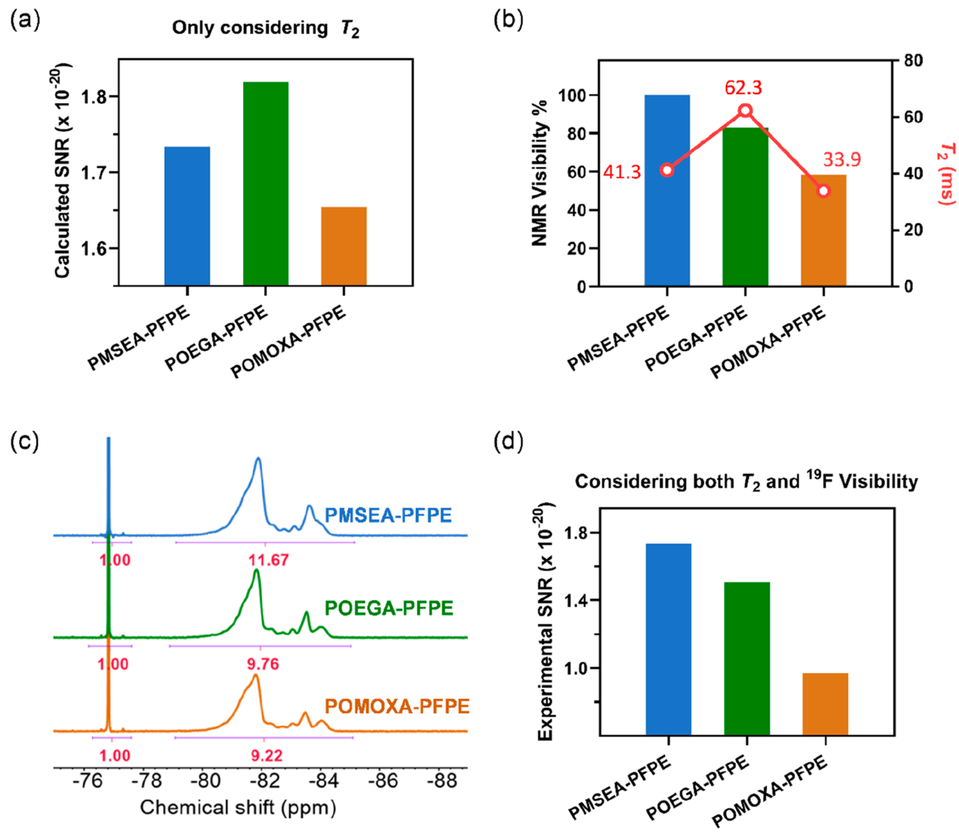

Figure 3. Quantitative spin-counting ^{19}F NMR experiments and calculated ^{19}F MRI SNRs. (a) The calculated SNRs of PMSEA−PFPE, POEGA−PFPE, and POMOXA−PFPE using eq 1 neglect the ^{19}F visibility. (b) ^{19}F NMR visibility and ^{19}F T_2. (c) ^{19}F NMR spectra of PMSEA−PFPE, POEGA−PFPE, and POMOXA−PFPE in PBS with a constant fluorine concentration of 6.8 mg/mL. Trifluoroethanol was used as the internal standard. (d) The calculated SNRs of PMSEA−PFPE, POEGA−PFPE, and POMOXA−PFPE using eq 1 with the inclusion of ^{19}F visibility.

fluorine atoms in the chemical structure of PFPE (Figure S3).[13,18,22] For instance, the most intense peak F1 at ∼−80 ppm is due to the difluoromethylene (2F, $-CF_2-$) and trifluoromethyl group (3F, $-CF_3$) from the PFPE segment of the copolymer. The NMR spectra confirm the successful synthesis of the three polymers, and the detailed structural characteristics of the polymers are summarized in Table 1.

The amphiphilic fluorinated block copolymers are expected to form core−shell assemblies driven by association of the hydrophobic PFPE segments in the aqueous solutions.[22,25] Dynamic light scattering (DLS) was used to confirm this hypothesis. The hydrodynamic diameters (D_h) observed from DLS of the three polymers were 9.3 nm for PMSEA−PFPE, 7.5 nm for POEGA−PFPE, and 8.0 nm for POMOXA−PFPE (Table 1). The D_h values were all well above the theoretical size for unimers (∼1 nm based on our previous reports[13,18,22]), indicating the formation of assemblies for all the three polymers in PBS solution.

The self-assembly behavior of the three polymers in aqueous solution was examined through molecular dynamics (MD) simulations. Figure 2a shows the initial molecular structure of PMSEA−PFPE, POEGA−PFPE, and POMOXA−PFPE. In Figure 2b, the MD simulation box was populated with 40 single polymer chains and filled with an aqueous solution containing 150 mM NaCl. We assume that equilibrium was reached for each polymer after a simulation time of 200 ns. All three polymers formed small-sized aggregates/micelles in aqueous solution with the hydrophobic PFPE as the core and hydrophilic segments within a surrounding shell. The multichain aggregates observed in MD simulations are consistent with the results obtained in the DLS measurements discussed above and are consistent with our previous reports.[17,22] In addition, the MD simulations reveal that the hydrophilic blocks adopt different conformations; i.e., the POMOXA chains adopt a much more rigid and extended conformation compared with the PMSEA and POEGA copolymers. This can be confirmed by the changes in average distance between terminal fragments of the hydrophilic chain and polymer backbone with simulation time (Figure 2c).

^{19}F MRI performance is highly sensitive to the segmental mobility and conformation of the fluorinated segments (i.e., PFPE in this case), and thus it is expected that the different assemblies revealed by MD simulations would impact NMR and MRI properties (Table 1).[13,23] ^{19}F NMR spin−lattice relaxation (T_1) and spin−spin (T_2) relaxation times of the three polymers were measured in PBS at a field strength of 9.4 T to evaluate chain mobility. The results in Table 1 indicate that the identity of the hydrophilic block can significantly affect the T_1 and T_2 relaxation times. To be more specific, POMOXA−PFPE has the shortest T_2, indicating the lowest chain mobility, which is suggested to be related to the rigid conformation of the hydrophilic segment shown in the MD simulations. In contrast, POEGA−PFPE has the longest T_2 relaxation time among the three polymers, indicating the highest segmental mobility of PFPE in solution. The expected ^{19}F MRI signal-to-noise ratio (SNR) of the three polymers was calculated with eq 1 using measured T_1 and T_2 relaxation times and the known fluorine content.[22] It can be concluded that the

https://doi.org/10.1021/acsmacrolett.2c00414
ACS Macro Lett. 2022, 11, 1195−1201

expected SNR of PMSEA−PFPE, POEGA−PFPE, and POMOXA−PFPE in arbitrary units is 1.73 × 10^{20}, 1.82 × 10^{20}, and 1.65 × 10^{20}, respectively (Figure 3a).

$$I = \nu N(F)\left[1 - 2\exp\left(\frac{-\left(T_R - \frac{T_E}{2}\right)}{T_1}\right) + \exp\left(\frac{-T_R}{T_1}\right)\right]\exp\left(\frac{-T_E}{T_2}\right) \quad (1)$$

In eq 1, I is the image intensity; ν is the ^{19}F NMR visibility factor; $N(F)$ is a measure of the fluorine concentration in the volume element of the image (based on 6.8 mg F); and T_R (1000 ms) and T_E (6 ms) are the pulse sequence repetition and echo times, respectively.

The expected ^{19}F MRI SNRs were calculated by assuming that all of the ^{19}F spins in the three polymers could be observed by MRI, i.e., were "NMR-visible". However, MD simulations indicate differences in self-assembly and especially the rigidity of the hydrophilic chain (Figure 2). Previously, a number of workers have reported that self-assembly including assembly of polymer chains above a lower critical solution temperature can lead to a reduction in NMR intensity of units with restricted molecular mobility.[26−29] Reduced molecular mobility results in enhance dipole−dipole interactions which can lead to such short T_2 relaxation times that the NMR signal becomes broadened into the spectral baseline.[30,31] Quantitative spin-counting ^{19}F NMR experiments of the polymers in PBS were used to determine the visibility of the ^{19}F spins. The contrast agent with PMSEA as the hydrophilic segment shows the highest ^{19}F visibility, and intensities in other spectra were normalized to this spectrum (Figure 3b). The POEGA and POMOXA block copolymers have much lower NMR visibility factor ν at 83% and 59% of that of PMSEA−PFPE, respectively (Figure 3b and 3c). Figure 3a and 3d shows the calculated imaging SNRs of the three polymers without and with the consideration of ^{19}F visibility. These plots highlight that NMR visibility and T_1 and T_2 relaxation times are all important parameters in determining imaging performance.

These observations are analogous to those of Thérien-Aubin and co-workers who examined the dynamics of poly(methyl acrylate) (PMA) chains tethered to the surface of cross-linked polystyrene (PS) nanoparticles.[32] Those workers varied the dynamics (stiffness) of the PS nanoparticle by changing the proportion of cross-linker divinylbenzene used in the miniemulsion polymerization of PS. The dynamics of the polymer chains within the PS core of the nanoparticles and within the PMA corona were examined from measurements of variable-temperature ^{1}H T_1 relaxation times. As in the current study, the dynamics of the more mobile chains, i.e., the PMA chains in the work of Thérien-Aubin, were significantly affected by changes in the dynamics of the attached chains, i.e., the PS core. In our work, the apparent rigid nature of the POMOXA reduces the local segmental mobility of the PFPE blocks to such an extent that a proportion of the ^{19}F spins is not NMR visible. Therefore, it can be concluded that the nature of the different types of hydrophilic side chain brushes, i.e., polymers of MSEA, OEGA, and OMOXA, significantly affects ^{19}F NMR properties, thus finally impacting the observed ^{19}F MRI intensity.

^{19}F MR images of solutions of the three polymers were obtained at different total fluorine concentrations to demonstrate the performance of our CAs. The ^{1}H RARE images illustrate the positions of the tubes in the resonator (Figure S4). For the ^{19}F MR images, the excitation and refocusing pulses were centered on the largest peak at approximately −80 ppm in the ^{19}F spectrum. As shown in Figure 4a, samples with higher concentrations of fluorine in solution show brighter ^{19}F MRI images.

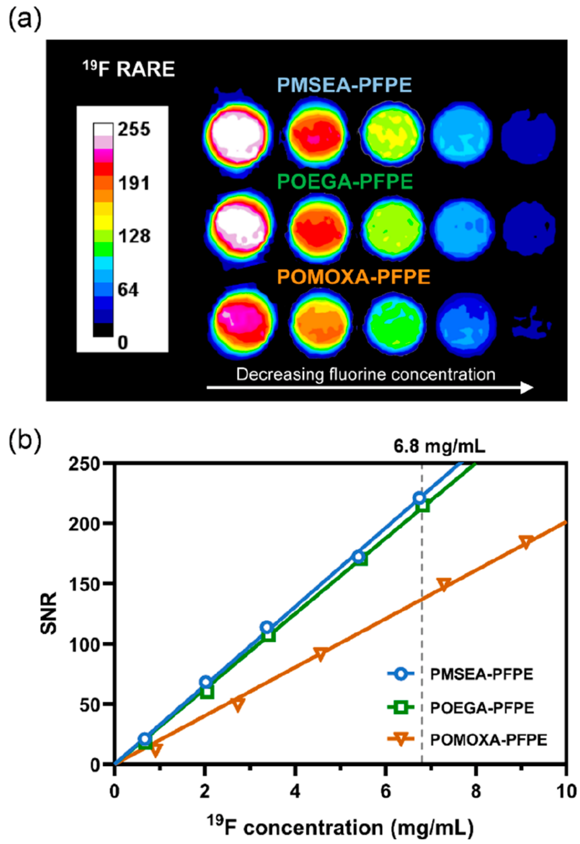

Figure 4. Concentration dependence of ^{19}F MRI. (a) ^{19}F MR images of PMSEA−PFPE, POEGA−PFPE, and POMOXA−PFPE in PBS. (b) Plots of ^{19}F MRI SNR as a function of fluorine concentration in solution. The SNR values were normalized according to the polymer concentration and the fluorine content of the polymer. The rapid acquisition with relaxation enhancement (RARE) sequence was used to measure the ^{19}F MR images of the solutions of the three different polymers.

For an ideal ^{19}F MRI CA to provide quantitative imaging information, the SNR should increase linearly with concentration.[33] The changes in ^{19}F MRI SNRs as a function of ^{19}F spin concentration from 1 to ∼10 mg/mL are shown in Figure 4b. The plots in Figure 4b show that the SNRs of all three polymers increase linearly with increasing fluorine concentration, indicating that the SNRs were only dependent on the fluorine concentration, and the relaxation times must not change significantly over this concentration range.

For the three polymers at the same fluorine concentration, the solution of PMSEA−PFPE had the strongest ^{19}F MRI intensity, followed by the POEGA−PFPE and POMOXA−PFPE. The differences in imaging intensity are more obvious at higher fluorine concentrations. To be more specific, as has been mentioned in Table 1, the imaging SNRs of PMSEA−PFPE, POEGA−PFPE, and POMOXA−PFPE are 222.0,

https://doi.org/10.1021/acsmacrolett.2c00414
ACS Macro Lett. 2022, 11, 1195−1201

213.5, and 136.9, respectively, at a ^{19}F concentration of 6.8 mg/mL. This observation is consistent with the SNRs calculated using eq 1 when taking both ^{19}F NMR visibility and NMR relaxation times into consideration (Figure 3d), highlighting that it is crucial to optimize both parameters to prepare ideal imaging candidates. The study also reveals the importance of the proper choice of hydrophilic segments to stabilize hydrophobic fluorinated segments in solution.[32]

In summary, a series of PFPE-containing block copolymers with three different hydrophilic segments were prepared, varying from 2-(methylsulfinyl)ethyl acrylate (MSEA), oligo-(ethylene glycol) methyl ether acrylate (OEGA), to oligo(2-methyl-2-oxazoline) acrylate (OMOXA). The effect of the hydrophilic chains on solution properties and ^{19}F NMR and MRI performance was investigated. The three polymers were observed to form assemblies in aqueous solution, confirmed by DLS and MD simulations, with the hydrophobic PFPE segments assembled as the core, surrounded by the hydrophilic blocks as the shell. As confirmed by MD simulations, the POMOXA chains have the most rigid conformation, leading to a short ^{19}F NMR spin−spin relaxation time (T_2), lower ^{19}F NMR spin visibility, and the least intense ^{19}F MRI signal from the PFPE segments. In contrast, the PMSEA and POEGA chains adopt a more flexible conformation, and corresponding improved NMR and MRI properties compared with polymers of POMOXA were observed. To be more specific, PMSEA−PFPE has a shorter ^{19}F NMR T_2 than POEGA−PFPE; however, the much higher ^{19}F spin visibility greatly improves its MRI performance. This work highlights the importance of proper choice of hydrophilic segments for preparing effective ^{19}F MRI imaging agents, providing important design parameters to improve imaging performance.

■ ASSOCIATED CONTENT

Supporting Information

The Supporting Information is available free of charge at https://pubs.acs.org/doi/10.1021/acsmacrolett.2c00414.

Materials and synthetic procedures, characterization methods, additional ^{1}H NMR and ^{19}F NMR spectra with assignments, as well as ^{1}H RARE MRI images of PMSEA−PFPE, POEGA−PFPE, and POMOXA−PFPE in PBS (PDF)

■ AUTHOR INFORMATION

Corresponding Authors

Cheng Zhang − *Australian Institute for Bioengineering and Nanotechnology and ARC Centre of Excellence in Convergent Bio-Nano Science and Technology, The University of Queensland, Brisbane, QLD 4072, Australia;* orcid.org/0000-0002-2722-7497; Email: c.zhang3@uq.edu.au

Andrew K. Whittaker − *Australian Institute for Bioengineering and Nanotechnology and ARC Centre of Excellence in Convergent Bio-Nano Science and Technology, The University of Queensland, Brisbane, QLD 4072, Australia;* orcid.org/0000-0002-1948-8355; Email: a.whittaker@uq.edu.au

Authors

Yiqing Wang − *Australian Institute for Bioengineering and Nanotechnology, The University of Queensland, Brisbane, QLD 4072, Australia*

Xiao Tan − *Australian Institute for Bioengineering and Nanotechnology and ARC Centre of Excellence in Convergent Bio-Nano Science and Technology, The University of Queensland, Brisbane, QLD 4072, Australia;* orcid.org/0000-0002-9278-6068

Adil Usman − *Australian Institute for Bioengineering and Nanotechnology and ARC Centre of Excellence in Convergent Bio-Nano Science and Technology, The University of Queensland, Brisbane, QLD 4072, Australia*

Yuhao Zhang − *Australian Institute for Bioengineering and Nanotechnology, The University of Queensland, Brisbane, QLD 4072, Australia;* orcid.org/0000-0001-5199-172X

Michał Sawczyk − *Department of Chemistry, University of Illinois at Chicago, Chicago, Illinois 60607, United States*

Petr Král − *Department of Chemistry, Department of Physics, and Department of Chemical Engineering, University of Illinois at Chicago, Chicago, Illinois 60607, United States; Department of Pharmaceutical Sciences, University of Illinois at Chicago, Chicago, Illinois 60612, United States;* orcid.org/0000-0003-2992-9027

Complete contact information is available at: https://pubs.acs.org/10.1021/acsmacrolett.2c00414

Author Contributions

CRediT: **Yiqing Wang** data curation (lead), formal analysis (lead), writing-original draft (lead); **Cheng Zhang** formal analysis (equal), methodology (equal), supervision (lead), writing-review & editing (equal); **Andrew K. Whittaker** supervision (equal), writing-review & editing (equal). **Xiao Tan** formal analysis (equal); **Adil Usman** methodology (equal); **Yuhao Zhang** formal analysis (equal); **Michał Sawczyk** methodology (equal), formal analysis (equal); **Petr Král** methodology (equal), formal analysis (equal).

Notes

The authors declare no competing financial interest.

■ ACKNOWLEDGMENTS

The authors acknowledge the Australian Research Council (CE140100036, DP0987407, DP110104299, DP130103774, DP180101221, DP210101496, LE0775684, LE0668517, and LE0882357) and the National Health and Medical Research Council (APP1021759, APP1046831, APP1107723, and APP1158026) for funding of this research. C.Z. acknowledges the National Health and Medical Research Council for his Early Career Fellowship (APP1157440). The Australian National Fabrication Facility, Queensland Node is acknowledged for access to some items of equipment.

■ REFERENCES

(1) Weissleder, R.; Mahmood, U. Molecular Imaging. *Radiology* **2001**, *219*, 316−333.

(2) Jafari, S. H.; Saadatpour, Z.; Salmaninejad, A.; Momeni, F.; Mokhtari, M.; Nahand, J. S.; Rahmati, M.; Mirzaei, H.; Kianmehr, M. Breast cancer diagnosis: Imaging techniques and biochemical markers. *J. Cell. Physiol.* **2018**, *233*, 5200−5213.

(3) Bogdanov, A A; Weissleder, R; Frank, H W; Bogdanova, A V; Nossif, N; Schaffer, B K; Tsai, E; Papisov, M I; Brady, T J A new macromolecule as a contrast agent for MR angiography: preparation, properties, and animal studies. *Radiology* **1993**, *187*, 701−706.

(4) Weissleder, R.; Tung, C.-H.; Mahmood, U.; Bogdanov, A. In vivo imaging of tumors with protease-activated near-infrared fluorescent probes. *Nat. Biotechnol.* **1999**, *17*, 375−378.

(5) Henkelman, R. M.; Stanisz, G. J.; Graham, S. J. Magnetization transfer in MRI: a review. *NMR Biomed.* **2001**, *14*, 57−64.
(6) Mizukami, S.; Takikawa, R.; Sugihara, F.; Hori, Y.; Tochio, H.; Wälchli, M.; Shirakawa, M.; Kikuchi, K. Paramagnetic Relaxation-Based ^{19}F MRI Probe To Detect Protease Activity. *J. Am. Chem. Soc.* **2008**, *130*, 794−795.
(7) Schmid, F.; Höltke, C.; Parker, D.; Faber, C. Boosting ^{19}F MRI—SNR efficient detection of paramagnetic contrast agents using ultrafast sequences. *Magn. Reson. Med.* **2013**, *69*, 1056−1062.
(8) Temme, S.; Grapentin, C.; Quast, C.; Jacoby, C.; Grandoch, M.; Ding, Z.; Owenier, C.; Mayenfels, F.; Fischer, J. W.; Schubert, R.; et al. Noninvasive imaging of early venous thrombosis by ^{19}F magnetic resonance imaging with targeted perfluorocarbon nano-emulsions. *Circulation* **2015**, *131*, 1405−1414.
(9) Waiczies, S.; Prinz, C.; Starke, L.; Millward, J. M.; Delgado, P. R.; Rosenberg, J.; Nazaré, M.; Waiczies, H.; Pohlmann, A.; Niendorf, T. Functional Imaging Using Fluorine (^{19}F) MR Methods: Basic Concepts. In *Preclinical MRI of the Kidney: Methods and Protocols*; Pohlmann, A., Niendorf, T., Eds.; Springer: US, 2021; pp 279−299.
(10) Ruiz-Cabello, J.; Barnett, B. P.; Bottomley, P. A.; Bulte, J. W. M. Fluorine (19F) MRS and MRI in biomedicine. *Des. Monomers Polym.* **2011**, *24*, 114−129.
(11) Taylor, N. G.; Chung, S. H.; Kwansa, A. L.; Johnson, R. R., III; Teator, A. J.; Milliken, N. J. B.; Koshlap, K. M.; Yingling, Y. G.; Lee, Y. Z.; Leibfarth, F. A. Partially Fluorinated Copolymers as Oxygen Sensitive ^{19}F MRI Agents. *Chem. Eur. J.* **2020**, *26*, 9982−9990.
(12) Ruiz-Cabello, J.; Barnett, B. P.; Bottomley, P. A.; Bulte, J. W. M. Fluorine (^{19}F) MRS and MRI in biomedicine. *NMR Biomed.* **2011**, *24*, 114−129.
(13) Fu, C.; Zhang, C.; Peng, H.; Han, F.; Baker, C.; Wu, Y.; Ta, H.; Whittaker, A. K. Enhanced Performance of Polymeric ^{19}F MRI Contrast Agents through Incorporation of Highly Water-Soluble Monomer MSEA. *Macromolecules* **2018**, *51*, 5875−5882.
(14) Zhang, C.; Yan, K.; Fu, C.; Peng, H.; Hawker, C. J.; Whittaker, A. K. Biological Utility of Fluorinated Compounds: from Materials Design to Molecular Imaging, Therapeutics and Environmental Remediation. *Chem. Rev.* **2022**, *122*, 167−208.
(15) Reis, M.; Gusev, F.; Taylor, N. G.; Chung, S. H.; Verber, M. D.; Lee, Y. Z.; Isayev, O.; Leibfarth, F. A. Machine-Learning-Guided Discovery of ^{19}F MRI Agents Enabled by Automated Copolymer Synthesis. *J. Am. Chem. Soc.* **2021**, *143*, 17677−17689.
(16) Fu, C.; Yu, Y.; Xu, X.; Wang, Q.; Chang, Y.; Zhang, C.; Zhao, J.; Peng, H.; Whittaker, A. K. Functional polymers as metal-free magnetic resonance imaging contrast agents. *Prog. Polym. Sci.* **2020**, *108*, 101286.
(17) Zhang, C.; Liu, T.; Wang, W.; Bell, C. A.; Han, Y.; Fu, C.; Peng, H.; Tan, X.; Král, P.; Gaus, K.; Gooding, J. J.; Whittaker, A. K. Tuning of the Aggregation Behavior of Fluorinated Polymeric Nanoparticles for Improved Therapeutic Efficacy. *ACS Nano* **2020**, *14*, 7425−7434.
(18) Zhang, C.; Sanchez, R. J. P.; Fu, C.; Clayden-Zabik, R.; Peng, H.; Kempe, K.; Whittaker, A. K. Importance of Thermally Induced Aggregation on ^{19}F Magnetic Resonance Imaging of Perfluoropolyether-Based Comb-Shaped Poly(2-oxazoline)s. *Biomacromolecules* **2019**, *20*, 365−374.
(19) Zhang, C.; Li, L.; Han, F. Y.; Yu, X.; Tan, X.; Fu, C.; Xu, Z. P.; Whittaker, A. K. Integrating Fluorinated Polymer and Manganese-Layered Double Hydroxide Nanoparticles as pH-activated ^{19}F MRI Agents for Specific and Sensitive Detection of Breast Cancer. *Small* **2019**, *15*, 1902309.
(20) Zhang, C.; Moonshi, S. S.; Wang, W.; Ta, H. T.; Han, Y.; Han, F. Y.; Peng, H.; Král, P.; Rolfe, B. E.; Gooding, J. J.; Gaus, K.; Whittaker, A. K. High F-Content Perfluoropolyether-Based Nanoparticles for Targeted Detection of Breast Cancer by ^{19}F Magnetic Resonance and Optical Imaging. *ACS Nano* **2018**, *12*, 9162−9176.
(21) Moonshi, S. S.; Zhang, C.; Peng, H.; Puttick, S.; Rose, S.; Fisk, N. M.; Bhakoo, K.; Stringer, B. W.; Qiao, G. G.; Gurr, P. A.; Whittaker, A. K. A unique ^{19} F MRI agent for the tracking of non phagocytic cells in vivo. *Nanoscale* **2018**, *10*, 8226−8239.
(22) Zhang, C.; Moonshi, S. S.; Han, Y.; Puttick, S.; Peng, H.; Magoling, B. J. A.; Reid, J. C.; Bernardi, S.; Searles, D. J.; Král, P.; Whittaker, A. K. PFPE-Based Polymeric ^{19}F MRI Agents: A New Class of Contrast Agents with Outstanding Sensitivity. *Macromolecules* **2017**, *50*, 5953−5963.
(23) Peng, H.; Blakey, I.; Dargaville, B.; Rasoul, F.; Rose, S.; Whittaker, A. K. Synthesis and evaluation of partly fluorinated block copolymers as MRI imaging agents. *Biomacromolecules* **2009**, *10*, 374−381.
(24) Wang, X.; Zhang, C.; Sawczyk, M.; Sun, J.; Yuan, Q.; Chen, F.; Mendes, T. C.; Howlett, P. C.; Fu, C.; Wang, Y. Ultra-stable all-solid-state sodium metal batteries enabled by perfluoropolyether-based electrolytes. *Nat. Mater.* **2022**, 1−9.
(25) Vukovic, L.; Khatib, F. A.; Drake, S. P.; Madriaga, A.; Brandenburg, K. S.; Kral, P.; Onyuksel, H. Structure and dynamics of highly PEG-ylated sterically stabilized micelles in aqueous media. *J. Am. Chem. Soc.* **2011**, *133*, 13481−13488.
(26) Plummer, R.; Hill, D. J.; Whittaker, A. K. Solution properties of star and linear poly (N-isopropylacrylamide). *Macromolecules* **2006**, *39*, 8379−8388.
(27) Zhang, C.; Peng, H.; Li, W.; Liu, L.; Puttick, S.; Reid, J.; Bernardi, S.; Searles, D. J.; Zhang, A.; Whittaker, A. K. Conformation transitions of thermoresponsive dendronized polymers across the lower critical solution temperature. *Macromolecules* **2016**, *49*, 900−908.
(28) Zhang, C.; Peng, H.; Puttick, S.; Reid, J.; Bernardi, S.; Searles, D. J.; Whittaker, A. K. Conformation of hydrophobically modified thermoresponsive poly (OEGMA-co-TFEA) across the LCST revealed by NMR and molecular dynamics studies. *Macromolecules* **2015**, *48*, 3310−3317.
(29) Zhang, C.; Peng, H.; Whittaker, A. K. NMR investigation of effect of dissolved salts on the thermoresponsive behavior of oligo (ethylene glycol)-methacrylate-based polymers. *J. Polym. Sci., Part A: Polym. Chem.* **2014**, *52*, 2375−2385.
(30) Reis, M. H.; Varner, T. P.; Leibfarth, F. A. The influence of residence time distribution on continuous-flow polymerization. *Macromolecules* **2019**, *52*, 3551−3557.
(31) Tan, X.; Zhong, J.; Fu, C.; Dang, H.; Han, Y.; Král, P.; Guo, J.; Yuan, Z.; Peng, H.; Zhang, C.; Whittaker, A. K. Amphiphilic Perfluoropolyether Copolymers for the Effective Removal of Polyfluoroalkyl Substances from Aqueous Environments. *Macromolecules* **2021**, *54*, 3447−3457.
(32) Kim, Y.-G.; Wagner, M.; Thérien-Aubin, H. l. Dynamics of soft and hairy polymer nanoparticles in a suspension by NMR relaxation. *Macromolecules* **2020**, *53*, 844−851.
(33) Tirotta, I.; Mastropietro, A.; Cordiglieri, C.; Gazzera, L.; Baggi, F.; Baselli, G.; Bruzzone, M. G.; Zucca, I.; Cavallo, G.; Terraneo, G.; et al. A superfluorinated molecular probe for highly sensitive in vivo ^{19}F-MRI. *J. Am. Chem. Soc.* **2014**, *136*, 8524−8527.

https://doi.org/10.1021/acsmacrolett.2c00414
ACS Macro Lett. 2022, 11, 1195−1201